OXFORD CENTRE FOR COLLABORATIVE APPLIED MATHEMATICS

Report Number 11/50

Wound healing angiogenesis: the clinical implications of a simple mathematical model

by

Jennifer A. Flegg, Helen M. Byrne, Mark B. Flegg, and D. L. Sean McElwain

Oxford Centre for Collaborative Applied Mathematics
Mathematical Institute
24 - 29 St Giles'
Oxford
OX1 3LB
England

Wound healing angiogenesis: the clinical implications of a simple mathematical model

Jennifer A. Flegg [a], Helen M. Byrne [b], Mark B. Flegg [c]
D. L. Sean McElwain [a],

[a] *School of Mathematical Sciences and Institute of Health and Biomedical Innovation, Queensland University of Technology, GPO Box 2434, Brisbane 4001, Australia*

[b] *School of Mathematical Sciences, University of Nottingham, Nottingham NG7 2RD, United Kingdom and Oxford Centre for Collaborative Applied Mathematics, Mathematics Institute, University of Oxford, Oxford, United Kingdom*

[c] *Oxford Centre for Collaborative Applied Mathematics, Mathematics Institute, University of Oxford, Oxford, United Kingdom*

Abstract

Nonhealing wounds are a major burden for health care systems worldwide. In addition, a patient who suffers from this type of wound usually has a reduced quality of life. While the wound healing process is undoubtedly complex, in this paper we develop a deterministic mathematical model, formulated as a system of partial differential equations, that focusses on an important aspect of successful healing: oxygen supply to the wound bed by a combination of diffusion from the surrounding unwounded tissue and delivery from newly-formed blood vessels. While the model equations can be solved numerically, the emphasis here is on the use of asymptotic methods to establish conditions under which new blood vessel growth can be initiated and wound-bed angiogenesis can progress. These conditions are given in terms of key model parameters including the rate of oxygen supply and its rate of consumption in the wound. We use our model to discuss the clinical use of treatments such as hyperbaric oxygen therapy, wound bed debridement, and revascularisation therapy that have the potential to initiate healing in chronic, stalled wounds.

Key words: chronic wound, hyperbaric oxygen therapy, numerical solution, asymptotic analysis
PACS:

Email addresses: j.flegg@qut.edu.au (Jennifer A. Flegg), helen.byrne@maths.ox.ac.uk (Helen M. Byrne), flegg@maths.ox.ac.uk (Mark B. Flegg), s.mcelwain@qut.edu.au (D. L. Sean McElwain).

1 Introduction

Lazarus et al. (1994) define a chronic wound to be one which either fails to proceed through an orderly and timely process to produce anatomic and functional integrity, or proceeds through the repair process without establishing a sustained anatomic and functional result. A recent estimate suggests that the US health care system spends in excess of US$25 billion annually treating patients with nonhealing wounds (Sen et al., 2009).

Wound healing is a highly-regulated and complex process, consisting of four stages (haemostasis, inflammation, proliferation and remodelling using the terminology of Grey and Harding (2006)) and requiring the coordination of the activites of many chemical and cellular species. Haemostasis typically lasts for a few hours and involves the control of blood loss in the damaged region. The inflammation stage lasts several days and coincides with inflammatory cell migration into the wound space and the release of chemical factors such as vascular endothelial growth factor (VEGF). These chemicals provide the stimulus that ultimately leads to the formation of new blood vessels (angiogenesis), an important step in the proliferative stage of healing. During this healing phase, there is a surge in the proliferation rate of fibroblasts, endothelial and epithelial cells and the rate at which collagen is deposited by fibroblasts (Jeffcoate et al., 2004). The final stage of healing sees the wound increase in tensile strength via remodelling of the extracellular matrix. The healing process is tightly regulated by many factors including oxygen supply and new capillary development. Grey and Harding (2006) provide a recent review of human wound healing and the factors that modulate it.

Most mathematical models of wound healing can be categorised as either population-based (or continuum) or cell-based (or discrete). An advantage of adopting a discrete approach is that it is possible to incorporate details that cannot easily be included within a continuum framework (see for example, Cumming et al., 2010). These features include cell-cell interactions, individual cell cycles, positioning of daughter cells after proliferation and discrete collagen fibres with individual orientations. However, continuum models are often more amenable to analysis than discrete ones. Geris et al. (2010) review *in silico* treatment strategies for wound healing together with some of the mathematical models that have been used to describe the healing process.

One of the earliest continuum models of angiogenesis in wound healing is a six-species, partial differential equation (PDE) model (chemoattractant, tips, oxygen blood vessels, fibroblasts and extracellular matrix) developed by Pettet et al. (1996b) to simulate the ingrowth of blood vessels. By performing numerical simulations they identified parameter sets for which healing stalled (by looking at mechanisms such as new capillary tip sprouting and chemoattractant production). In other work, Pettet et al. (1996a) used perturbation methods to derive approximate expressions for the wavespeed of a soft-tissue healing wound while Gaffney et al. (2002) applied travelling wave analysis to a simple PDE model to estimate the wavespeed of the healing front. More recently, Schugart et al. (2008) developed a seven-species model of angiogenesis (the six species from the model by Pettet et al. (1996b) and additionally macrophages) in order to investigate the role of oxygen tension in cutaneous wound healing. Schugart et al. used their model to

generate several predictions. For example, they claim that wounds will not heal in extremely hypoxic environments and that the use of hyperbaric oxygen therapy may stimulate angiogenesis. These predictions are consistent with earlier experimental work (Hopf et al., 2005; Kim et al., 2007). Xue et al. (2009) extended the model of Schugart et al. (2008) by incorporating mechancal effects in that they treated the ECM as a viscoelastic material. To the best of our knowledge, Xue et al. (2009) is the first mechanochemical model of wound healing angiogenesis. Vermolen (2009) has developed a system of nonlinear reaction-diffusion equations for oxygen, growth factors, epidermal cells and capillaries and simulated healing in two spatial dimensions. While these models give considerable insight into wound healing, they do not lend themselves to the derivation of simple expressions relating the success (or failure) of wound healing to the system parameters.

There have been several discrete models of the related phenomenon of tumour-induced angiogenesis, including important work by Chaplain and Anderson (1999) that is based on a finite difference approximation of PDEs and Bauer et al. (2007) who use the cellular Potts model framework. It is worth noting that wound healing angiogenesis is a regulated process whereas tumour-induced angiogenesis is uncontrolled. For a detailed review of mathematical models of tumour-induced angiogenesis, see Mantzaris et al. (2004).

In this paper, we develop a mathematical model based on the assumption that revascularization of the wound bed is the rate-limiting step in successful healing. While other processes, such as ECM deposition and remodelling, are undoubtedly important, restoration of a good oxygen supply is vital for the repair of damaged

tissue (Hunt and Gimbel, 2002). Our aim is to derive simple criteria, in terms of the model parameters, for which successful healing will be initiated. We then use these criteria to assess common treatment therapies such as debridement, revascularistion, and hyperbaric oxygen therapy (Thackham et al., 2008; Flegg et al., 2009).

In the next section we develop our mathematical model and present the governing partial differential equations. In Section 3, we present typical numerical simulations while in Section 4 we analyse the model and identify regions of parameter space in which we predict healing will succeed or fail. In Section 5, we discuss the implications of our results and make suggestions for further work.

2 Description of the Mathematical Model

Our mathematical model comprises three partial differential equations: one for the oxygen concentration, w, one for the capillary tip density, n, and one for the blood vessel density, b. The equations are based on the principle of mass conservation and are stated below in dimensional form. For simplicity, we consider a one-dimensional wound whose edge is located at $x = 0$ and whose centre lies at $x = L$, with symmetry about $x = L$. It is worth noting that in our one-dimensional model, the capillary tip density is effectively averaged in the plane perpendicular to the direction in which the healing front advances. The model is based on the previous work by Pettet et al. (1996a,b).

2.1 The Model Equations

Oxygen concentration, $w(x,t)$;

We assume that oxygen diffuses through the wound space with diffusivity D_w, is supplied locally by the blood vessels at rate $k_2 b$ and is consumed by the tissue at rate $k_4 w$, where D_w, k_2 and k_4 are non-negative constants. Combining these ideas we deduce the equation describing the evolution of the oxygen concentration:

$$\frac{\partial w}{\partial t} = D_w \frac{\partial^2 w}{\partial x^2} + k_2 b - k_4 w. \tag{1a}$$

Implicit in Eq. (1a) is the assumption that the oxygen concentration in the fully healed tissue, which we denote by w_{healed}, is maintained at a baseline level at which supply and demand balance so that, $w_{\text{healed}} = k_2 b_0 / k_4$ where b_0 denotes the blood vessel density in unwounded tissue.

Capillary tip density, $n(x,t)$;

The evolution of the capillary tip profile is assumed to be dominated by chemotaxis, tip-sprouting from vessels and tip regression so that

$$\frac{\partial n}{\partial t} = \chi \frac{\partial}{\partial x}\left(n \frac{\partial w}{\partial x} \right) + k_5 b H(w - w_L) H(w_H - w) - k_6 n. \tag{1b}$$

In Eq. (1b) $H(x)$ is the Heaviside function which we define as follows: $H(x) = 1$ for $x \geq 0$ and $H(x) = 0$ otherwise. Several different approaches to modelling capillary tip chemotaxis within the wound space have been proposed. Typically, it is

assumed that a chemoattractant, such as VEGF, is produced by macrophages or other inflammatory cells during early wound healing and in response to hypoxia. Capillary tips then migrate up spatial gradients of the chemoattractant (see for example, Pettet et al. (1996a,b); Schugart et al. (2008)). Gaffney et al. (2002) used a different (but equivalent) approach, modelling the migration of endothelial cells (ECs) down spatial gradients in the blood vessel density.

Since VEGF production appears to be triggered by hypoxia (Al-Waili and Butler, 2006), we anticipate that the oxygen and VEGF profiles will be complementary. Hence, migration up the spatial gradients in VEGF will be equivalent to migration down spatial gradients of oxygen (in a similar way to that in which Gaffney et al. (2002) model endothelial cell migration down the spatial gradients in blood vessel density). With this in mind, we model the chemotactic motion of capillary tips as in Eq. (1b), with a constant chemotactic coefficient, χ. While the model could be extended to include new species, namely macrophages and VEGF, we argue that our approach is sufficient to incorporate the salient features of angiogenesis, such as oxygen-regulated ingrowth of new vessels. We assume further that if the oxygen concentration is too high (that is, hyperoxia, $w > w_H$) or too low (that is, chronic hypoxia, $w < w_L$) then no capillary tips will be produced while for intermediate values (i.e, $w_L < w < w_H$) they sprout from existing vessels at rate $k_5 b$. Finally, we assume that tip death occurs at rate $k_6 n$, which is independent of the local oxygen concentration. We remark that capillary tip loss due to anastomosis with other tips and blood vessels could be modelled by including terms proportional to nb and n^2 in Eq. (1b), for which Edelstein (1982) provide details: here we neglect such

effects and assume instead that apoptosis dominates capillary tip removal. The way we model chemotaxis and capillary tip production and their dependence on the oxygen concentration distinguishes this work from previous models.

Blood vessel density, $b(x,t)$;

The blood vessel density $b(x,t)$ is assumed to evolve as follows:

$$\frac{\partial b}{\partial t} = -\chi n \frac{\partial w}{\partial x} + k_3 b(b_0 - b). \tag{1c}$$

In Eq. (1c) we follow Balding and McElwain (1985), using the "snail trail" concept to model the deposition of blood vessels by the migrating capillary tips. This approach, which was originally developed by Edelstein et al. (1983) to investigate fungal growth, assumes that new blood vessels are laid down behind the advancing capillary tips at rate nv where $v = -\chi \dfrac{\partial w}{\partial x} > 0$ is the speed with which the capillary tips move (see Eq. (1b)). Remodelling of the newly formed blood vessels is accomplished through the logistic term, with carrying capacity $b = b_0$ and growth rate k_3. This remodelling term is similar to those employed by other authors, including Gaffney et al. (2002).

Boundary and initial conditions

The following boundary and initial conditions are imposed to close Eqs. (1):

$$\left.\frac{\partial w}{\partial x}\right|_{x=0} = \left.\frac{\partial w}{\partial x}\right|_{x=L} = 0, \quad n(0,t) = 0, \tag{2a}$$

$$w(x,0)=\begin{cases}\dfrac{k_2 b_0}{k_4} & 0<x<\varepsilon\\ 0 & \varepsilon<x\le L,\end{cases}\qquad b(x,0)=\begin{cases}b_0 & 0<x<\varepsilon\\ 0 & \varepsilon<x\le L,\end{cases}\qquad n(x,0)=0,\ 0\le x\le L. \tag{2b}$$

At the wound centre, $x = L$, a zero-flux condition is imposed on the oxygen concentration due to the assumed spatial symmetry of the wound domain. We assume that there are no capillary tips at the wound edge, $x = 0$, and that oxygen levels equilibrate rapidly with uninjured levels so that the oxygen flux there will be zero. We further assume that initially there are no tips within the wound space, the blood vessel density is that of normal tissue within a certain distance from the wound edge ($0 < x < \varepsilon$) and that the wound is oxygenated throughout this vascularised region such that demand for oxygen (at rate $k_4 w$) balances supply (at rate $k_2 b_0$). We assume that the width of the wound margin, ε, that separates the wounded and healthy tissues is small so that $\varepsilon \ll L$.

2.2 Nondimensionalisation of the Model

We nondimensionalise the model by taking

$$w = \bar{w}w^*,\ x = \bar{x}x^*,\ n = \bar{n}n^*,\ b = \bar{b}b^* \quad \textit{and} \quad t = \bar{t}t^*,$$

where the asterisks denote dimensionless variables and the bars denote characteristic values of the variables. We choose

$$\bar{b} = b_0, \bar{n} = \frac{b_0}{\bar{x}} \quad \text{and} \quad \bar{t} = \frac{1}{k_3 b_0}.$$

We do not specify a characteristic value for the oxygen concentration since we want to vary $k_2 b$ and $k_4 w$, the rates of supply and and demand for oxygen, in order to investigate how these mechanisms govern the success or failure of the healing of a wound. The characteristic lengthscale, $\bar{x}$ is also left arbitrary since we want the wound centre to be far enough away from the advancing healing front so that the symmetry condition at the wound centre does not effect the numerical solution. We also introduce the following dimensionless parameters:

$$k_2^* = \frac{k_2}{k_3 \bar{w}} \quad k_4^* = \frac{k_4}{k_3 b_0} \quad k_5^* = \frac{k_5 \bar{x}}{k_3 b_0} \quad k_6^* = \frac{k_6}{k_3 b_0} \quad w_H^* = \frac{w_H}{\bar{w}}$$

$$w_L^* = \frac{w_L}{\bar{w}} \quad \varepsilon^* = \frac{\varepsilon}{\bar{x}} \quad D_w^* = \frac{D_w}{k_3 b_0 \bar{x}^2} \quad \chi^* = \frac{\chi \bar{w}}{k_3 b_0 \bar{x}^2} \quad L^* = \frac{L}{\bar{x}}.$$

Under the above scaling and omitting the asterisks for notational simplicity, Eqs. (1) and (2) transform to give the following system of PDEs and boundary and initial conditions:

$$\frac{\partial w}{\partial t} = D_w \frac{\partial^2 w}{\partial x^2} + k_2 b - k_4 w, \tag{3a}$$

$$\frac{\partial n}{\partial t} = \chi \frac{\partial}{\partial x}\left(n \frac{\partial w}{\partial x} \right) + k_5 b H(w - w_L) H(w_H - w) - k_6 n, \tag{3b}$$

$$\frac{\partial b}{\partial t} = -\chi n \frac{\partial w}{\partial x} + b(1 - b), \tag{3c}$$

$$\left.\frac{\partial w}{\partial x}\right|_{x=0} = \left.\frac{\partial w}{\partial x}\right|_{x=L} = 0, \quad n(0,t) = 0, \tag{4a}$$

$$w(x,0) = \begin{cases} \dfrac{k_2}{k_4} & 0 < x < \varepsilon \\ 0 & \varepsilon < x \leq L, \end{cases} \qquad b(x,0) = \begin{cases} 1 & 0 < x < \varepsilon \\ 0 & \varepsilon < x \leq L, \end{cases} \qquad n(x,0) = 0,\ 0 \leq x \leq L. \tag{4b}$$

3 Numerical Results

Eqs. (3) and (4) are solved numerically using a finite volume method, with a Roe-flux limiting approach employed to discretise the chemotaxis term in Eq. (3b) (Thackham et al., 2009). Unless otherwise stated, the dimensionless parameters are fixed at the following values:

$$D_w = 10, \qquad \chi = 1, \qquad k_2 = 150, \quad k_4 = 150, \quad k_5 = 100,$$

$$k_6 = 100, \quad w_H = 0.5, \quad w_L = 0.3, \quad \varepsilon = 0.1, \qquad L = 2.$$

We stress that this choice of parameter values is employed for illustrative purposes only, since our main goal is to derive conditions, in terms of arbitrary but reasonable, parameter values, for the initiation of successful healing. While the above values are used to generate a typical simulation in which successful healing occurs, order of magnitude estimates for each system parameter can be obtained from existing mathematical models in which parameter values were derived from the experimental literature (Flegg et al., 2009)

The spatio-temporal evolution of the three species during a typical simulation of successful healing is shown in Fig. 1. Oxygen diffuses into the wound space from the surrounding healthy tissue and establishes a local oxygen gradient, down which capillary tips migrate. As the capillary tips move into the wound, they leave behind them a network of new blood vessels, which deliver additional oxygen to the wound and allow the capillary tips and blood vessels to move further into the wound. In this way, we observe a steadily advancing wave of invasion from left (wound edge) to right (wound centre) in the capillary tip and blood vessel profiles. When the

capillary tips reach the centre of the wound, they are removed via anastomosis. Hence, the initial wound space will eventually be completely revascularised and oxygen levels returned to normal, indicating the completion of the healing process.

Dimensionless parameter	Relative change	Percentage healed
baseline	–	17%
D_c	$\uparrow \times 5$	No healing
	$\downarrow \times 5$	34%
χ	$\uparrow \times 5$	92%
	$\downarrow \times 5$	$< 1\%$
k_2	$\uparrow \times 5$	No healing
	$\downarrow \times 5$	No healing
k_4	$\uparrow \times 5$	No healing
	$\downarrow \times 5$	No healing
k_5	$\uparrow \times 5$	75%
	$\downarrow \times 5$	2%
k_6	$\uparrow \times 5$	$< 1\%$
	$\downarrow \times 5$	90%

Table 1
Summary of the predicted changes that occur if the baseline set of parameters are varied by a factor of 5. The percentage healed represents the percentage of the domain that has a dimensionless blood vessel density exceeding 0.5 at time $t = 5$.

We performed a sensitivity analysis by increasing and decreasing each of the system parameters by a factor of 5 (see Table 1). We run the full numerical simulation of Eqs. (3) and (4) until $t = 5$ and compare the outputs for the different parameter values at this time by calculating the percentage of the wound domain ($0 < L < 2$) which has healed. Here, we define the healed tissue to be when the dimensionless blood vessel density reaches a threshold value of 0.5. This analysis revealed two processes are critical to successful wound healing: the supply of oxygen from the blood vessels ($k_2 b$) and the consumption of oxygen ($k_4 w$). Guided

by these results, the (k_2, k_4) parameter space is explored in detail in the next section. The baseline parameter set is 17% healed at time $t = 5$, however all of the changes to parameters k_2 and k_4 result in stalled healing (see Table 1).

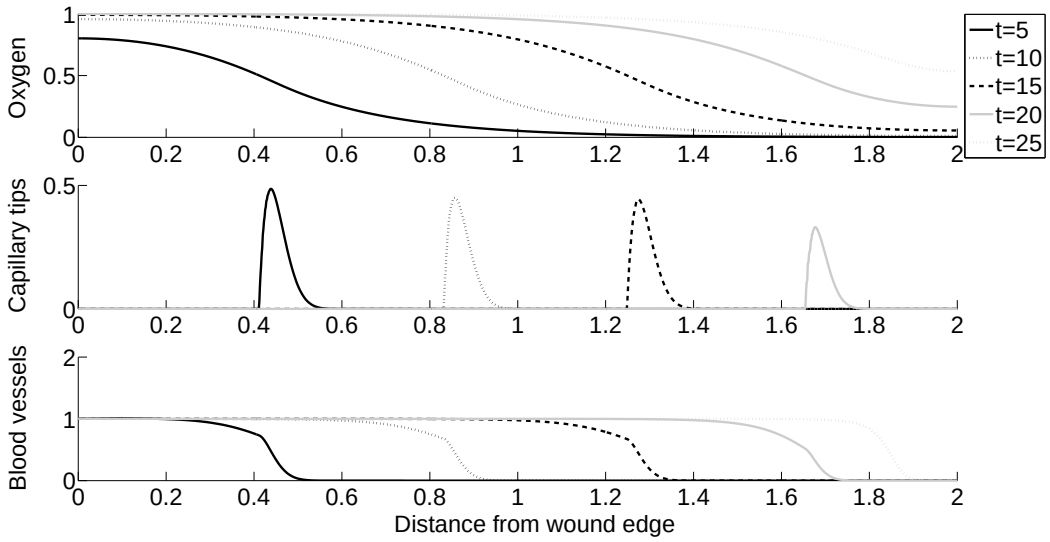

Fig. 1. Results from numerical solution of Eqs. (3) subject to the conditions (4) showing the distributions of oxygen, capillary tips and blood vessels at dimensionless times of $t = 5, 10$ and 15. The solution profiles evolve rapidly to fixed profiles which travel from left to right at constant speed until the wound space is completely revascularised and oxygen level returns to normal. Parameter values are: $D_w = 10$, $\chi = 1$, $k_2 = 150$, $k_4 = 150$, $k_5 = 100$, $k_6 = 100$, $w_H = 0.5$, $w_L = 0.3$, $\varepsilon = 0.1$, $L = 2$. Using a value of $k_3 b_0 = 1.3$/day used previously (Flegg et al., 2009), a dimensionless time of 25 coressponds to approximately 19 days.

Using our model it is possible to simulate situations for which healing stalls because angiogenesis fails to occur. For example, fixing all parameters, except k_2, at the values used in Fig. 1, healing stalls if the rate at which oxygen is supplied to the wound through the blood vessels is decreased by a factor of 5, from $k_2 = 150$ to $k_2 = 30$ (see Figure 2). Healing fails because the wound space becomes so severely hypoxic that the oxygen concentration everywhere is too low to stimulate tip production. Similaryly, fixing all parameters, except k_4, at the values used in Fig. 1, healing stalls if the oxygen consumption rate is increased, from $k_2 = 150$, by a factor of 5. Healing fails because the wound space is hyperoxic in the region where

existing blood vessls are and hence no capillary tip production can occur.

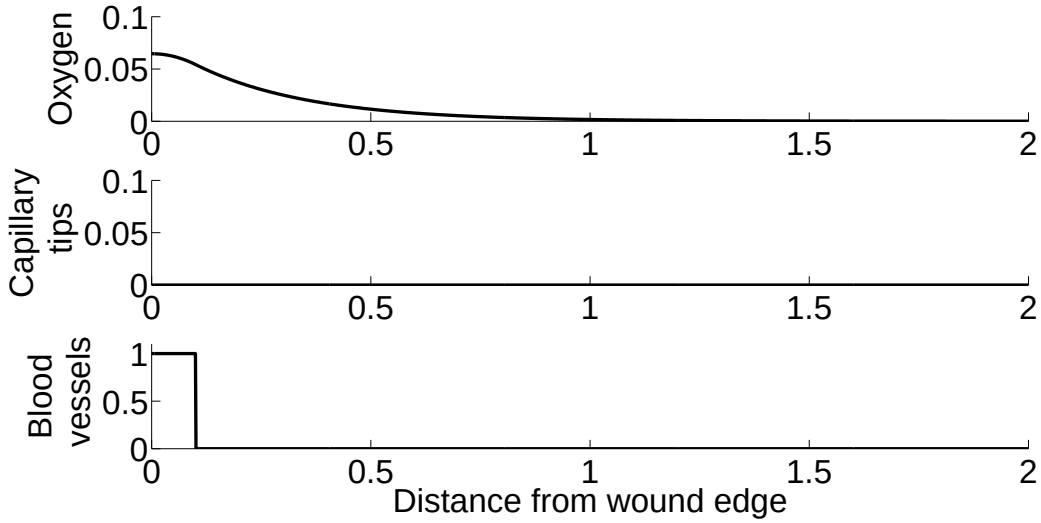

Fig. 2. Results from numerical solution of Eqs. (3) subject to the conditions (4) showing the distributions of oxygen, capillary tips and blood vessels at dimensionless times of $t = 5$. The solution profiles show that no capillary tips are produced within the wound. Parameter values are: $D_w = 10$, $\chi = 1$, $k_2 = 30$, $k_4 = 150$, $k_5 = 100$, $k_6 = 100$, $w_H = 0.5$, $w_L = 0.3$, $\varepsilon = 0.1$, $L = 2$.

4 Establishing Necessary Conditions for Initiating Healing

The early behaviour is known to be an accurate predictor of the ultimate success or failure of a wound to heal (Margolis et al., 2004). In this section we investigate whether the success or failure of healing can be predicted from the early time dynamics of our model. We can then use our results to predict those types of nonhealing wounds that would benefit from treatment. Guided by our numerical simulations we consider cases for which the parameters D_w, k_2, k_4, k_5 and k_6 are large. More precisely, we introduce a small parameter $0 < \delta \ll 1$ and assume

$$D_w = \frac{\hat{D_w}}{\delta^2}, k_2 = \frac{\hat{k_2}}{\delta^2}, k_4 = \frac{\hat{k_4}}{\delta^2}, k_5 = \frac{\hat{k_5}}{\delta}, k_6 = \frac{\hat{k_6}}{\delta},$$

where the hats represent $\mathcal{O}(1)$ quantities. We investigate the early time behaviour by rescaling on the short timescale $t = \delta\tau$ so that Eqs. (3) transform to give

$$\delta\frac{\partial w}{\partial \tau} = \hat{D_w}\frac{\partial^2 w}{\partial x^2} + \hat{k_2}b - \hat{k_4}w, \tag{5a}$$

$$\frac{\partial n}{\partial \tau} = \delta\chi\frac{\partial}{\partial x}\left(n\frac{\partial w}{\partial x}\right) + \hat{k_5}bH(w - w_L)H(w_H - w) - \hat{k_6}n, \tag{5b}$$

$$\frac{\partial b}{\partial \tau} = -\delta\chi n\frac{\partial w}{\partial x} + \delta b(1 - b). \tag{5c}$$

Henceforth, we omit the hats for notational simplicity. We seek approximate solutions to Eqs. (5) which are regular power series expansions in δ so that, for example,

$$w = w_0(x, \tau) + \delta w_1(x, \tau) + \mathcal{O}(\delta^2).$$

The solution of the leading order equations yields the following approximate expressions for the oxygen concentration (w_0), the capillary tip density (n_0) and the blood vessel density (b_0):

$$w_0(x) = \begin{cases} \dfrac{k_2}{k_4}\left(1 - \dfrac{\sinh\left(\theta(L-\varepsilon)\right)}{\sinh\left(\theta L\right)}\cosh\left(\theta x\right)\right) & \text{for} \quad 0 \le x < \varepsilon, \\ \dfrac{k_2}{k_4}\dfrac{\sinh\left(\theta\varepsilon\right)}{\sinh\left(\theta L\right)}\cosh\left(\theta(L-x)\right) & \text{for} \quad \varepsilon < x \le L, \end{cases} \tag{6a}$$

where $\theta^2 = \dfrac{k_4}{D_w}$ and we have demanded continuity of oxygen and its first spatial derivative at $x = \varepsilon$.

$$b_0 = b(x, 0) = H(\varepsilon - x), \tag{6b}$$

$$n_0(\tau) = \begin{cases} 0 & \text{for} \quad 0 \leq x < x_{left}(\tau), \\ \dfrac{k_5}{k_6}\left(1 - e^{-k_6\tau}\right) & \text{for} \quad x_{left}(\tau) < x < x_{right}(\tau), \\ 0 & \text{for} \quad x_{right}(\tau) < x \leq L. \end{cases} \tag{6c}$$

where $x_{left}(\tau)$ and $x_{right}(\tau)$ are the left and right-most extremes of the wound in which capillary tip production occurs.

On this early time scale, the leading order response of capillary tips is production in the region $x_{left}(\tau) < x < x_{right}(\tau)$ and no response outside of this region. At leading order the blood vessels remain at their initial distribution while for $\varepsilon < x < L$, the dominant processes for oxygen are diffusion and consumption and for $0 < x < \varepsilon$ diffusion, supply and consumption dominate.

We note here that this early time approximation for the capillary tips is discontinuous at $x = x_{left}(\tau)$ and $x = x_{right}(\tau)$ for $\tau > 0$. Here $x = x_{left}(\tau)$ and $x = x_{right}(\tau)$ mark the left and right-most extremes of the wound in which capillary tip production occurs (that is, the oxygen concentration is such that capillary tip production occurs in $x_{left}(\tau) < x < x_{right}(\tau)$). Their locations will change with time, τ. Since we are investigating the early time behaviour of the model we shall suppose that $x_{left}(\tau) = x_{left}(0) + \delta x_{left,1}(\tau) + \mathcal{O}(\delta^2)$, with a similar expression for $x_{right}(\tau)$. If we focus on the leading order behaviour so that $x_{left}(\tau) \approx x_{left}(0)$ and $x_{right}(\tau) \approx x_{right}(0)$ and the boundaries between the healing zone and outer regions move slowly at early times, then it is straightforward to show that six different cases can arise depending on the initial oxygen concentrations at $x = x_{left}(0)$ and $x = x_{right}(0)$. These cases are summarised in

Table 4 and are discussed in turn below.

We note that without explicitly solving for the $\mathcal{O}(\delta)$ correction terms we cannot determine whether the leading order behaviour remains valid for large τ. However, in Figure 3 we present numerical evidence that confirms our early time approximations are in good agreement with the numerical solutions for large times.

Case Number	Condition/s	$x_{left}(0)$	$x_{right}(0)$	Healing initiated
1	$w_0(0) \leq w_L$, $\forall x \in (0, L)$	—	—	No
2	$w_0(\epsilon) \leq w_H$, $\forall x \in (0, \varepsilon)$	—	—	No
3	$w_0(\epsilon) \leq w_L \leq w_0(0) \leq w_H$	0	x_L	Yes
4	$w_L \leq w_0(\epsilon) \leq w_0(0) \leq w_H$	0	ε	Yes
5	$w_0(\epsilon) \leq w_L < w_H \leq w_0(0)$	x_H	ε	Yes
6	$w_L \leq w_0(\epsilon) \leq w_H \leq w_0(0)$	x_H	x_L	Yes

Table 2
Summary of the six possible cases that can arise and predictions about the onset of angiogenesis.

Case 1: Chronic hypoxia. If $w_0(0) < w_L$ then **healing does not occur** because the oxygen concentration throughout the wound is too low to stimulate angiogenesis. Using Eq. (6a) we deduce that a necessary condition for this case to arise is that the parameters satisfy:

$$\frac{k_2}{k_4} < w_L \left(1 - \frac{\sinh\left(\theta(L-\varepsilon)\right)}{\sinh\left(\theta L\right)}\right)^{-1},$$

where $\theta = \sqrt{\dfrac{k_4}{D_w}}$. In this case,

$$n(x,t) = n(x,0) = 0,\ b(x,t) = b(x,0) = H(\varepsilon - x),\ w(x,t) \to w_0(x) \text{ as } t \to \infty.$$

Case 2: Chronic hyperoxia. If $w_0(\varepsilon) \geq w_H$ then **healing does not occur**

because the oxygen concentration is everywhere too high to stimulate angiogenesis. A necessary condition for this case to arise is:

$$\frac{k_2}{k_4} > \frac{w_H \sinh(\theta L)}{\sinh(\theta\varepsilon)\cosh(\theta(L-\varepsilon))}.$$

In Case 2,

$$n(x,t) = n(x,0) = 0, b(x,t) = b(x,0) = H(\varepsilon - x),\ w(x,t) \to w_0(x) \text{ as } t \to \infty.$$

Case 3: Tip production is restricted by wound edge ($x = 0$) and oxygen falling below lower threshold value. If $w_L \leq w_0(0) \leq w_H$ and $w_0(\varepsilon) \leq w_L$ then **healing is successful** and tip production takes place on the interval $x \in [0, x_L]$, where $0 < x_L < \varepsilon$ and $w_0(x = x_L) = w_L$. Using Eq. (6a), it is straightforward to show that this case will arise if the system parameters are such that:

$$w_L\left(1 - \frac{\sinh(\theta(L-\varepsilon))}{\sinh(\theta L)}\right)^{-1} \leq \frac{k_2}{k_4} \leq \min\left[\frac{w_L \sinh(\theta L)}{\sinh(\theta\varepsilon)\cosh(\theta(L-\varepsilon))}, w_H\left(1 - \frac{\sinh(\theta(L-\varepsilon))}{\sinh(\theta L)}\right)^{-1}\right].$$

Case 4: Tip production occurs throughout the entire wound margin. If $w_L \leq w_0(\varepsilon) \leq w_0(0) \leq w_H$ then **healing is successful** and tip production takes place on the interval $x \in [0, \varepsilon]$. This case arises if the parameters satisfy:

$$\frac{w_L \sinh(\theta L)}{\sinh(\theta\varepsilon)\cosh(\theta(L-\varepsilon))} \leq \frac{k_2}{k_4} \leq w_H\left(1 - \frac{\sinh(\theta(L-\varepsilon))}{\sinh(\theta L)}\right)^{-1}.$$

Case 5: Tip production is initiated by oxygen concentration falling

below upper threshold value and halted by wound margin ($x = \varepsilon$). If $w_0(0) \geq w_H$ and $w_L \leq w_0(\varepsilon) \leq w_H$ then **healing is successful** and tip production occurs for $x \in [x_H, \varepsilon]$, where $0 < x_H < \varepsilon$ and $w_0(x = x_H) = w_H$. The conditions on the model parameters for this case to arise are as follows:

$$\max\left[\frac{w_L \sinh(\theta L)}{\sinh(\theta\varepsilon)\cosh(\theta(L-\varepsilon))}, w_H\left(1 - \frac{\sinh(\theta(L-\varepsilon))}{\sinh(\theta L)}\right)^{-1}\right] \leq \frac{k_2}{k_4} \leq \frac{w_H \sinh(\theta L)}{\sinh(\theta\varepsilon)\cosh(\theta(L-\varepsilon))}.$$

Case 6: Tip production is initiated and restricted only by oxygen concentration falling below upper threshold and lower oxygen threshold values, respectively. If $w_0(0) \geq w_H$ and $w_0(\varepsilon) \leq w_L$ then **healing is successful** and tip production takes place on the interval $x \in [x_H, x_L]$, where $0 < x_H < x_L < \varepsilon$, $w_0(x = x_L) = w_L$ and $w_0(x = x_H) = w_H$. This case arises if the parameters satisfy:

$$w_H\left(1 - \frac{\sinh(\theta(L-\varepsilon))}{\sinh(\theta L)}\right)^{-1} \leq \frac{k_2}{k_4} \leq \frac{w_L \sinh(\theta L)}{\sinh(\theta\varepsilon)\cosh(\theta(L-\varepsilon))}.$$

We now use the inequalities derived above to classify (k_2, k_4) parameter space into distinct regions, based on whether or not healing is successful and further sub-characterised by the six cases defined in Table 2. With the exception of k_2 and k_4, we hold fixed all other system parameters so that: $w_L = 0.3$, $w_H = 0.5$, $L = 2$, $D_w = 10$ and $\varepsilon = 0.1$. For this choice of parameter values and for the range of values of k_2 and k_4 considered, only cases 1-5 were observed. It was possible to observe case 6 by increasing the lower oxygen threshold from $w_L = 0.3$ to $w_L = 0.45$, and holding w_H, L and D_w fixed. Figure 3(a) shows the predicted

regions of unsuccessful healing (cases 1 and 2) and successful healing (cases 3, 4 and 5). Cases 1 and 2 are undesirable extremes where healing fails due to insufficient and excessive oxygen, respectively. While cases 2, 3 and 4 lead ultimately to successful wound healing, our analysis does not enable us to determine which case gives rise to the fastest healing. We therefore constructed numerical solutions to the full problem (see Eqs. 3 and 4) for a range of values of k_2 and k_4 and estimated the healing speed from the numerical solutions. By following the location in the wound space at which the blood vessel density was 10% of its normal levels (that is, $b = 0.1$ in dimensionless terms) and then averaging over the simulation until $0 \leq t \leq 5$ (see Figure 3(b)). The wavespeed calculated in this way was found to be comparable to the speed of the points where $w = w_H$ and $w = w_L$. That is, by comparing the results in Figures 3(a) and 3(b) we can see that the small-time analysis is a good predictor of the success of healing for $t \gg 0$.

Fig. 4 shows plots of the numerical speed (calculated from the full numerical simulation of Eqs. 3 and 4) when keeping k_4 constant and varying k_2 over $[0, 350]$ (upper subplot) and in the lower plot, keeping k_2 constant and varying k_4 over $[0, 250]$. Fig. 4 clearly shows that the healing speed for k_2 and k_4 that lie in cases 1 and 2 are indeed 0 (in agreement with our analysis) and that the other cases yield non-zero speeds. The increase in k_2 increases the oxygen concentration so that capillary tip production can occur and allows the wound to heal.

(a)

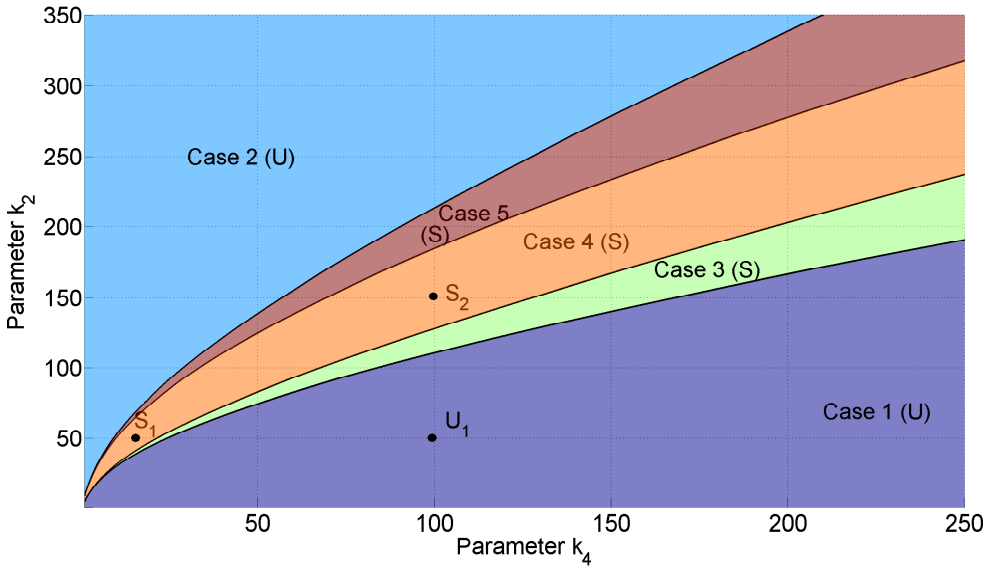

(b)

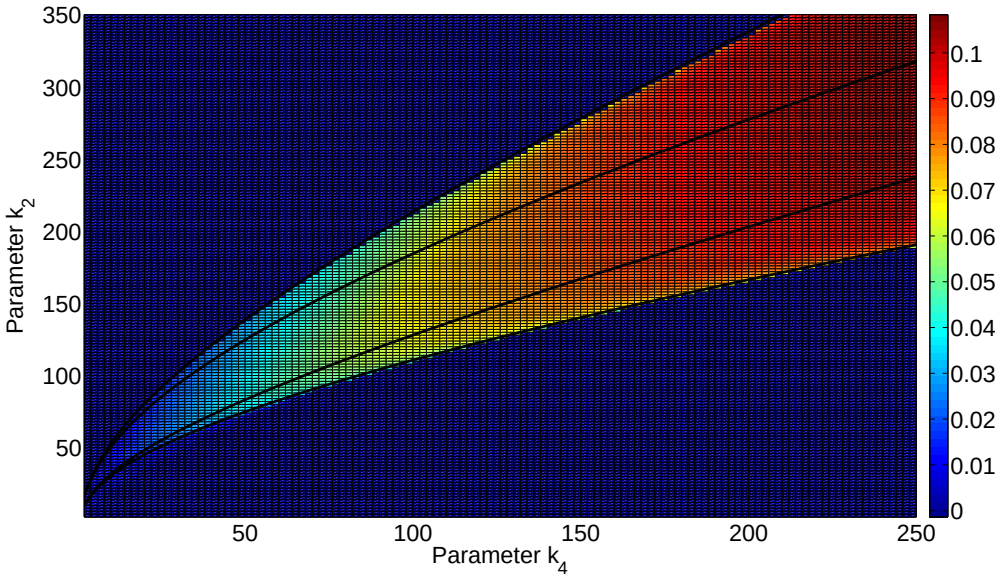

Fig. 3. (a) Sketch of (k_2,k_4) parameter space, showing, for a particular set of parameter values, that there are 5 distinct healing regimes arise. See Table 2 for a description of these cases. Cases 1 and 2 give unsuccessful healing (U), while cases 3-5 yield successful healing (S). Parameter values: $w_L = 0.3$, $w_H = 0.5$, $L = 2$, $D_w = 10$ and $\varepsilon = 0.1$. For a description of the meaning of the points labelled U_1, S_1 and S_2, see Section 5. (b) Contour plot obtained by numerical solution of original model out to $t = 5$ (see Eqs 3 and 4) showing how the wavespeed changes as (k_2,k_4) vary.

5 Clinical Implications and Discussion

= Regardless of their aetiology, many chronic wounds are hypoxic and this can compromise healing (Mathieu, 2002). We can use our model to compare the

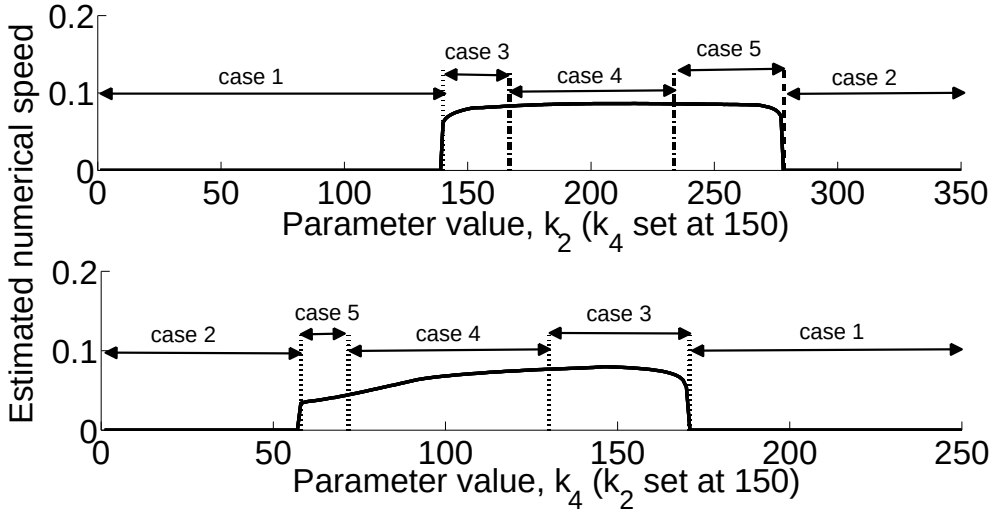

Fig. 4. Plot of numerical speed versus the parameter k_2 that characterises oxygen supply from the blood vessels (upper subplot) and changing k_4 that characterises the oxygen consumption rate of the healing tissue (lower subplot). The value of the parameter k_4 is set at 150 for the upper subplot and k_2 is set at 150 for the lower subplot. The speed is estimated from the full numerical simulation of Eqs. 3 and 4. Both subplots show that healing only occurs in a range of the parameter values.

efficacy of different treatments that are routinely used to treat nonhealing wounds. We note that if a wound has stalled due to a lack of oxygen (see point U_1 in Figure 3), it should be possible to initiate healing by either sufficiently increasing the oxygen supply rate, as characterised by the parameter k_2 (the point S_2) or sufficiently decreasing the oxygen consumption rate, as characterised by the parameter k_4 (the point S_1).

Diabetic wounds are often low in oxygen due to an over-abundance of oxygen-consuming inflammatory cells and bacteria. A common treatment for these types of wounds is debridement where the infected tissue is removed (Lerman et al., 2003). This will effectively decrease the local oxygen consumption rate, k_4. Provided that the decrease in k_4 is sufficient to shift the wound condition from its current position in Case 1 of (k_2, k_4) parameter space into one of the Cases 3-5, but not into Case 2 parameter space, then our model predicts that the treatment

will yield successful healing. The simulation results presented in Fig. 5 illustrate the effect of an intermittent increase in oxygen supply (that is, increasing k_2). We observe that when the oxygen supply is at its initial level (for times in the range $0 < t < 1$) no healing occurs. An increase in oxygen supply (for $1 < t < 2$) is sufficient to initiate a propagating healing front. When the oxygen supply is returned to its original level (for $2 < t$), the healing speed does not return to its initial speed. That is, the wound continues to heal after the treatment is completed.

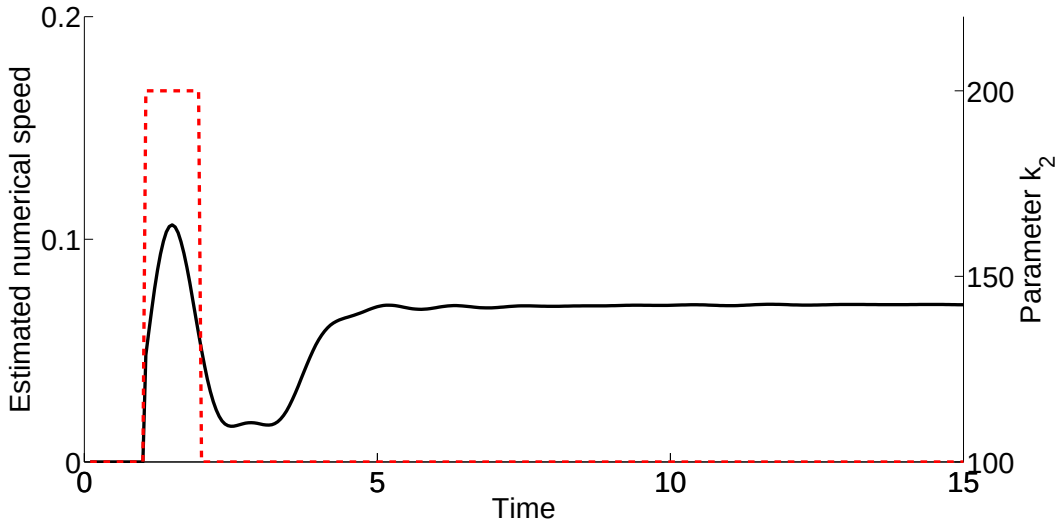

Fig. 5. Plot of numerical speed versus time. The value of the parameter k_2 is initally 100 (for $0 < t < 1$), then its value is doubled to 200 (for $1 < t < 2$) and then its value is returned to the initial value of 100. The speed is estimated from the full numerical simulation of Eqs. 3 and 4.

Arterial leg wounds are also associated with low oxygen levels. However this is typically due to poor arterial flow and a common treatment is revascularisation surgery wherein the arterial flow is improved (Grey et al., 2006). In this case, revascularisation will effectively increase the oxygen supply rate parameter, k_2. Provided that the increase in k_2 is sufficiently large that the critical parameters are in the parameter space covered by Cases 3-5 (but not increased too much so that the system enters the Case 2 parameter regime), we predict that treatment will

successfully stimulate healing.

Hyperbaric oxygen therapy aims to correct chronic hypoxia by allowing patients to breathe oxygen at high pressure (typically 2.4 atmospheres) for approximately 90 minutes each day over a time period of about six weeks (see Thackham et al., 2008 for a comprehensive review). Hyperbaric oxygen therapy is often used to treat diabetic patients with stalled chronic wounds (Thackham et al., 2008; Flegg et al., 2009) and attempts to facilitate healing by increasing the peripheral oxygen supply to the wound bed. We can incorporate HBOT into our model by assuming that during its application the oxygen supply increases so that $k_2^{\mathrm{HBOT}} = k_2 + \Delta k_2$, where $\Delta k_2 > 0$. The early time analysis presented in Section 4 suggests that HBOT, modelled in the way described above, will have a positive effect on the stalled wound if the treatment causes a sufficient rise in the oxygen supply rate, k_2. However, care is needed in specifying a suitable treatment protocol since an exposure that increases k_2 too much will prevent healing due to excessive oxygen in the wound space (causing the system parameters to enter the region associated with Case 2 in Figure 3(a))

Previous theoretical studies of wound healing (such as that by Schugart et al. (2008) and Flegg et al. (2010)) have focussed on more detailed models which permit a more thorough investigation of the effect of interactions between chemicals and cells. In this paper we have developed a 3-species mathematical model that captures the essential elements of wound healing angiogenesis, while being simple enough to allow analytical analysis. Specifically, we have derived conditions, in terms of key model parameters, for which healing will be successful

and others for which it will fail. The results from our analysis compare very well with the numerical solution of the full set of PDEs. We can use our model to make predictions about the efficacy for treatments of chronic wounds. We are now in a position to tailor our model to specific wound aetiologies and even specific patients and use it to compare the outcomes of different therapies. We plan to extend the current model to higher spatial dimensions and investigate the other possible benefits and impacts that HBOT has on the healing process (such as reactive oxygen species, hypoxia inducible factor pathway and nitric oxide).

Acknowledgments

This work was supported by the award of a doctoral scholarship to JAF from the Institute of Health and Biomedical Innovation at Queensland University of Technology and was funded by Australian Research Council's Discovery Projects funding scheme (project number DP0878011) (JAF). This research was carried out while HMB was visiting Queensland University of Technology, funded by the Institute of Health and Biomedical Innovation and the Discipline of Mathematical Sciences. Computational resources and services used in this work were provided by the HPC and Research Support Unit, QUT. This publication was based on work supported in part by Award No KUK-C1-013-04, made by King Abdullah University of Science and Technology (KAUST).

References

Al-Waili, N., Butler, G., 2006. Effects of Hyperbaric Oxygen on Inflammatory Response to Wound and Trauma: Possible Mechanism of Action. The Scientific World 6, 425–441.

Balding, D., McElwain, D., 1985. A mathematical model of tumour-induced capillary growth. J Theor Biol 114, 53–73.

Bauer, A., Jackson, T., Jiang, Y., 2007. A cell-based model exhibiting branching and anastomosis during tumor-induced angiogenesis. Biophysical journal 92 (9), 3105–3121.

Chaplain, M., Anderson, A., 1999. Modelling the growth and form of capillary networks. John Wiley & Sons Ltd, Ch. 13, pp. 225–249.

Cumming, B., McElwain, D., Upton, Z., 2010. A mathematical model of wound healing and subsequent scarring. Journal of The Royal Society Interface 7 (42), 19.

Edelstein, L., 1982. The propagation of fungal colonies: a model for tissue growth* 1. Journal of Theoretical Biology 98 (4), 679–701.

Edelstein, L., Hadar, Y., Chet, I., Henis, Y., Segel, L., 1983. A model for fungal colony growth applied to Sclerotium Reolfsii. J. Gen. Microbiol. 129, 1873–1881.

Flegg, J. A., McElwain, D. L. S., Byrne, H. M., 2010. Mathematical model of hyperbaric oxygen therapy applied to chronic diabetic wounds. Bulletin of Mathematical Biology Accepted.

Flegg, J. A., McElwain, D. L. S., Byrne, H. M., Turner, I. W., 07 2009. A three species model to simulate application of hyperbaric oxygen therapy to chronic

wounds. PLoS Comput Biol 5 (7), e1000451.

Gaffney, E., Pugh, K., Maini, P., Arnold, F., 2002. Investigating a simple model of cutaneous wound healing angiogenesis. J. Math. Biol. 45(4), 337–374.

Geris, L., Schugart, R., Van Oosterwyck, H., 2010. In silico design of treatment strategies in wound healing and bone fracture healing. Philosophical Transactions of the Royal Society A: Mathematical, Physical and Engineering Sciences 368 (1920), 2683.

Grey, J., Harding, K. (Eds.), 2006. ABC of Wound Healing. Blackwell Publishing.

Grey, J., Harding, K., Enoch, S., 2006. Venous and Arterial Leg Ulcers. BMJ 332(7537), 347–350.

Hopf, H., Gibson, J., Angeles, A., Constant, J., Feng, J., Rollins, M., Hussain, M., Hunt, T., 2005. Hyperoxia and Angiogenesis. Wound Repair and Regeneration 13(6), 558–564.

Hunt, T., Gimbel, M., 2002. Hyperbaric surgery. Best Publishing Company, Ch. Hyperbaric oxygen and wound healing, pp. 439–459.

Jeffcoate, W., Price, P., Harding, K., 2004. Wound Healing and Treatments for People with Diabetic Foot Ulcers. Diabetes Metab Res Rev 20 Suppl 1, S78–589.

Kim, P., Heilala, M., Steinberg, J., Weinraub, G., 2007. Bioengineered Alternative Tissues and Hyperbaric Oxygen in Lower Extremity Wound Healing. Clinics in Podiatric Medicine and Surgery 24 (3), 529–546.

Lazarus, G., Cooper, D., Knighton, D., Margolis, D., Percoraro, R., Rodeheaver, G., Robson, M., 1994. Definitions and guidelines for assessment of wounds and evaluation of healing. Wound Rep Reg 2, 165–170.

Lerman, O., Galiano, R., Armour, M., Levine, J., Gurtner, G., 2003. Cellular

Dysfunction in the Diabetic Fibroblast. American Journal of Pathology 162(1), 303–312.

Mantzaris, N., Webb, S., Othmer, H., 2004. Mathematical modeling of tumor-induced angiogenesis. J Math Biol 49, 111–187.

Margolis, D., Allen-Taylor, L., Hoffstad, O., Berlin, J., 2004. The accuracy of venous leg ulcer prognostic models in a wound care system. Wound Repair and Regeneration 12 (2), 163–168.

Mathieu, D., 2002. Hyperbaric Surgery. Best Publishing Company, Ch. 12: Hyperbaric Oxygen Therapy in the Management of Non-healing Wounds, pp. 317–339.

Pettet, G. J., Byrne, H. M., McElwain, D. L. S., Norbury, J., 1996a. A model of wound healing angiogenesis in soft tissue. Mathematical Biosciences 136(1), 35–63.

Pettet, G. J., Chaplain, M. A. J., McElwain, D. L. S., Byrne, H. M., 1996b. On the role of angiogenesis in wound healing. Proc. R. Soc. Lond. B 263(1376), 1487–1493.

Schugart, R., Friedman, A., Zhao, R., Sen, C., 2008. Wound angiogenesis as a function of tissue oxygen tension: A mathematical model. Proceedings of the National Academy of Sciences 105 (7), 2628–2633.

Sen, C., Gordillo, G., Roy, S., Kirsner, R., Lambert, L., Hunt, T., Gottrup, F., Gurtner, G., Longaker, M., 2009. Human skin wounds: A major and snowballing threat to public health and the economy. Wound Repair and Regeneration 17 (6), 763–771.

Thackham, J., McElwain, D., Long, B., 2008. The use of hyperbaric oxygen

therapy to treat chronic wounds: a review. Wound Repair and Regeneration 16, 321–330.

Thackham, J., McElwain, D., Turner, I., 2009. Computational approaches to solving equations arising from wound healing. Bulletin of Mathematical Biology 71 (1), 211 – 246.

Vermolen, F., 2009. Simplified Finite-Element Model for Tissue Regeneration with Angiogenesis. Journal of Engineering Mechanics 135, 450.

Xue, C., Friedman, A., Sen, C., 2009. A mathematical model of ischemic cutaneous wounds. Proceedings of the National Academy of Sciences 106 (39), 16782.

RECENT REPORTS

27/11	Particle trapping and banding in rapid solidification	Elliot Peppin
28/11	Growth of confined cancer spheroids: a combined experimental and mathematical modelling approach	Loessner Flegg Byrne Hall Moroney Clements McElwain Hutmacher
29/11	Floating carpets and the delamination of elastic sheets	Wagner Vella
30/11	Numerical Study of Liquid Crystal Elastomers by a Mixed Finite	Luo Calderer
31/11	The indentation of pressurized elastic shells: From polymeric capsules to yeast cells	Vella Ajdari Vaziri Boudaoud
32/11	Wrinkling of pressurized elastic shells	Vella Ajdari Vaziri Boudaoud
33/11	Data assimilation using bayesian filters and B-spline geological models	Duan Farmer Hoteit Lu Moroz
34/11	Review of nonlinear Kalman, ensemble and particle filtering with application to the reservoir history matching problem	Luo Hoteit Duan Wang
35/11	Modelling a Tethered Mammalian Sperm Cell undergoing Hyperactivation	Curtis Kirkman-Brown Connolly Gaffney
36/11	A simple mathematical model for investigating the effect of cluster roots on plant nutrient uptake	Zygalakis Roose
37/11	Frequency jumps in the planar vibrations of an elastic beam	Neukirch Frelat Goriely Maurini
38/11	Ice-lens formation and con nement-induced supercooling in soils and other colloidal materials	Style Cocks Peppin Wettlaufer
39/11	An asymptotic theory for the re-equilibration of a micellar surfactant solution	Griffiths Bain

42/11	An efficient implementation of an implicit FEM scheme for fractional-in-space reaction-diffusion equations	Burrage Hale Kay
43/11	Coupling fluid and solute dynamics within the ocular surface tear film: a modelling study of black Line osmolarity	Zubkov Breward Gaffney
44/11	A prototypical model for tensional wrinkling in thin sheets	Davidovitch Schroll Vella Adda-Bedia Cerda
45/11	A fibrocontractive mechanochemical model of dermal wound closure incorporating realistic growth factor	Murphy Hall Maini McCue McElwain
46/11	A two-compartment mechanochemical model of the roles of transforming growth factor β and tissue tension in dermal wound healing	Murphy Hall Maini McCue McElwain
47/11	Effects of demographic noise on the synchronization of a metapopulation in a fluctuating environment	Lai Newby Bressloff
48/11	High order weak methods for stochastic differential equations based on modified equations	Abdulle Cohen Vilmart Zygalakis
49/11	The kinetics of ice-lens growth in porous media	Style Peppin

Copies of these, and any other OCCAM reports can be obtained from:

Oxford Centre for Collaborative Applied Mathematics
Mathematical Institute
24 - 29 St Giles'
Oxford
OX1 3LB
England
www.maths.ox.ac.uk/occam